Unimolecular Decomposition of Formic Acid in the Gas Phase—On the Ratio of the Competing Reaction Channels

Ko Saito,[†] Takanori Shiose,[†] Osamu Takahashi,[†] Yoshiaki Hidaka,[‡] Fuhito Aiba,[‡] and Kiyohiko Tabayashi*[,†]

Department of Chemistry, Graduate School of Science, Hiroshima University, Higashi-Hiroshima 739-8526, Japan, and Department of Chemistry, Faculty of Science, Ehime University, Bunkyo-cho, Matsuyama 790-8577, Japan

Received: October 28, 2004; In Final Form: April 24, 2005

The thermal decomposition of formic acid was reinvestigated in the gas phase using two types of shock tubes. It was confirmed that the unimolecular decomposition proceeds through a main channel of dehydration (k_1) and a minor decarboxylation channel (k_2). This result is in good agreement with our previous study (*J. Chem. Phys.* **1984**, *80*, 4989). Furthermore, it was confirmed that the dehydration process is in the second-order region and that the decarboxylation is in the falloff region, in the temperature range of 1300−2000 K and over the total density of $(0.5-2.5) \times 10^{-5}$ mol cm^{-3}. The experimental ratios between the two channels, k_2/k_1, are compared with those of theoretical calculations by conventional transition state theory and the Rice−Ramsperger−Kassel−Marcus theory.

Introduction

The unimolecular decomposition of formic acid is well-known to occur through the following molecular elimination pathways:

$$\mathrm{HCOOH\ (+M)} \rightarrow \mathrm{CO + H_2O\ (+M)} \quad (1)$$

$$\rightarrow \mathrm{CO_2 + H_2\ (+M)} \quad (2)$$

The decomposition of formic acid has been investigated both experimentally[1−8] and theoretically[9−15] for a long time. Among the experimental studies, two different investigations have been reported using a shock tube at high temperatures. Hsu et al.[4] monitored the time-dependent CO concentration by IR absorption with a CO laser. They obtained comparable second-order rate constants for these competitive channels, $k_{1,0}$ and $k_{2,0}$, where $k_{n,0}$ is the second-order rate constant of channel n defined by $k_{n,0} = k_n$/[M], and determined that the Arrhenius parameters for the two channels were log $A_{1,0}$ (cm^3 mol^{-1} s^{-1}) = 15.36, $E_{a1,0}$ = 50 kcal mol^{-1} and log $A_{2,0}$ (cm^3 mol^{-1} s^{-1}) = 16.18, $E_{a2,0}$ = 57 kcal mol^{-1}. On the basis of the results, they estimated the comparable threshold energies for the two reaction channels to be E_1 = 62−65 kcal mol^{-1} and E_2 = 65−68 kcal mol^{-1}, respectively. They also confirmed that other channels such as the production of radical species via a simple bond scission were not important as the initiation reactions. One year later, Saito et al.[5] reported another experiment under the shock conditions similar to the experiment by Hsu et al. Saito et al. measured the decomposition rate by monitoring the reactant and product behavior of the IR emission intensities. The total amount of the CO_2 production was found to be less than 5% of the initial reactant at the end of the reaction where almost all the reactants have disappeared. They concluded that the decomposition actually proceeded via the dehydration and that the rate constant for the decalboxylation, $k_{2,0}$, was about 2 orders of magnitude smaller than $k_{1,0}$ on the basis of the Rice−Ramsperger−Kassel−Marcus (RRKM) theory. The Arrhenius parameters of the second-order rate constant for channel 1 were evaluated to be log $A_{1,0}$ (cm^3 mol^{-1} s^{-1}) = 14.32 and $E_{1,0}$ = 40.4 kcal mol^{-1}. The potential barrier height (E_2) for the decalboxylation was estimated to be 20−30 kcal mol^{-1} higher than that of the dehydration. Several experimental works on the laser-induced decomposition of formic acid[6−8] have favored the predominance of the dehydration channel in the decomposition of formic acid.

Many theoretical investigations have been performed for the energy barrier heights of the two channels. Earlier studies[5,9] of ab initio molecular orbital (MO) calculations have shown the difference in barrier heights for the two channels to be about 20 kcal mol^{-1} due to the low-level approximations. Recent progress in quantum chemistry has made it possible to estimate more reliable potential energy surfaces. Typically, Ruelle et al.,[10,11] Goddard et al.,[12] and Francisco[13] obtained almost the same barrier heights (within a few kcal mol^{-1}) for the two channels, although different approximations were used. It is not curious that they came to suspect our previous experimental results, especially our shock tube work,[5] where the decalboxylation is a few percent of the total decomposition. As a consequence, they received the results of Hsu et al.[4]

Water-catalyzed reactions, which may largely lower the potential barrier on the reaction path, have been studied theoretically by several researchers.[16−18] It seems, however, that the catalyzed reaction is still the minor one in the homogeneous thermal decomposition at high temperatures. Another possible reaction is a direct decomposition from a formic acid dimer that exists about 30% in the gas phase when ca. 1 Torr (1 Torr = 133.322 Pa) of formic acid is kept at room temperature.

As described previously, many investigators have so far been interested in the thermal decomposition of formic acid. Even at the present stage, there still remains ambiguity on the branching ratio between the two competing channels. The main purpose of this study is to check the previous shock tube works.

* Corresponding author. Phone: +81-82-424-7406; fax: +81-82-424-0727; e-mail: tabayasi@sci.hiroshima-u.ac.jp.
[†] Hiroshima University.
[‡] Ehime University.

10.1021/jp045072h CCC: $30.25
Published on Web 06/01/2005

Here, we also discuss the experimental and theoretical results reported hitherto.

Experimental Procedures

Two shock tubes were used in the present study. The first was a standard type of 9.4 cm i.d.[5,19] The test section of the tube was evacuated to less than 2×10^{-6} Torr by a 6 in. diffusion pump before each run. A pair of CaF_2 or MgF_2 disks was mounted on the tube wall at the observing position, 2 cm apart from the end plate for reflected shock experiments. When experiments were performed behind the incident waves, an additional tube of about 16 cm in length was attached to the end flange. The decomposition of formic acid was monitored by observing the time-resolved IR radiation from CO (4.63 ± 0.09 μm) and CO_2 (4.23 ± 0.09 μm), and the dissociation of the formic acid dimer was monitored at 5.66 ± 0.05 μm, which is the C═O stretching of the monomeric formic acid. The IR emission was detected by an MCT (mercury−cadmium−tellurium) photoconductive element (1×1 mm^2) cooled at 77 K. Usually, a slit of 1.0 mm in width was set outside of the window, and the MCT element was set at the position 80 mm apart from the slit. The output signals from the MCT and pressure transducer mounted on the same position of the windows were recorded simultaneously by a digital oscilloscope. The time constant of the optical detection systems was about 10 μs. The shock-heated gas mixture for each run was taken out to a 1 L glass cylinder and analyzed for the production yields of CO and CO_2 by using an IR gas analyzer (Shimadzu, CGT-7000) and a gas detector (Kitagawa Style, Model 370S).

Sample gases were treated in a manner similar to the previous experiment.[5] The concentration of dimer $(HCOOH)_2$ was estimated to be 10−20% of gaseous formic acid at room temperature depending on the sample pressure.[19] This value cannot be neglected in the present experiment because the decomposition reaction might also proceed from the dimer molecule as suggested by several investigators. Therefore, we examined the behavior of the dimer at high temperatures.

The second shock tube was a magic-hole type.[20−23] The product gas mixtures heated by the single pulse method were extracted into a preevacuated vessel (50 cm^3) through a valve near the end plate and analyzed by serially connected three gas-chromatographs (Shimadzu), each of them having a thermal conductivity detector. The standard gas sample prepared for the calibration of CO and CO_2 concentration by Seitetsu Kagaku was used for the identification and quantification of each product. The quantification of each product was carried out using Ar as a reference material. The amounts of the products were determined within an accuracy of ±4%. An effective heating time t_e (reaction time), defined as the time between the arrival of the reflected shock wave and the 80% point of fall from the reflected shock pressure, was determined with an accuracy of ±5% using the method described previously.[20−22] The t_e values at the representative temperatures were determined from the relationship between the observed t_e and reflected shock temperature. The t_e values obtained at the representative temperatures 1000, 1100, 1200, 1300, 1400, 1500, and 1600 K were 812, 916, 1021, 1125, 1229, 1333, and 1437 μs, respectively. The concentrations of CO and CO_2 determined by gas chromatography were compared with those simulated, assuming that the reaction was frozen perfectly at the end of the effective heating time. The t_e values increased with increasing the temperature under our experimental conditions. To obtain the shock wave with lower temperatures, the concentration ratio of H_2/N_2 of the driver gas was lowered. As a result, the heating time was shortened by lowering the shock temperature. The cooling rates under our experimental conditions were about 830 and 500 K/ms at 1500 and 1000 K, respectively.

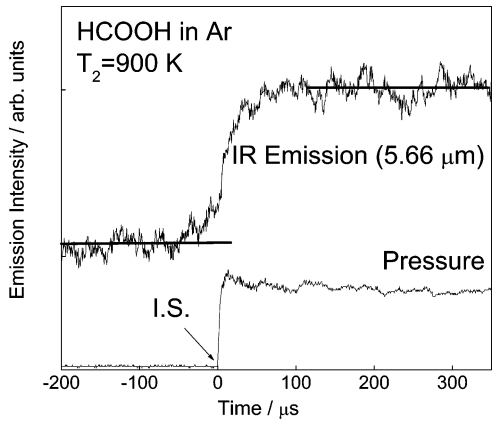

Figure 1. Typical IR emission at 5.66 μm that corresponds to formic acid monomer. Conditions behind the indent wave are $T_2 = 900$ K and $\rho_2 = 5.0 \times 10^{-6}$ mol cm^{-3}. I.S. indicated the incident shock front.

The computer simulation procedure of the shock-heated reactions was essentially the same as described previously.[20−24] The routine of the computations was a Gear-type integration of a set of differential equations describing the chemical kinetics under the constant density conditions for a reflected shock wave. Reverse reactions were automatically included in the computer program through equilibrium constants computed from thermochemical data. Thermochemical data for Ar, CO, H_2, H_2O, and CO_2 were adopted from the JANAF tables,[25] and those for HCOOH were given from ref 26.

To estimate the rotationally averaged microcanonical rate constants $k(E)$ for two competed channels, the RRKM calculations were performed using a code UNIMOL developed by Gilbert et al.[27] Structural information for the ground and transition states were adopted from the results of Takahashi et al.,[14] and other parameters were from the experimental conditions. The temperature and pressure dependence have been calculated by employing the second part of the UNIMOL algorithm and using Lennard−Jones parameters adjusted for formic acid. More specifically, the Lennard−Jones diameter σ_{AB} for reactant-bath gas was taken to be equal to 4.04 Å, and the Lennard−Jones well depth ϵ_{AB} was equal to 183.9 K using the parameters $\sigma_{Ar} = 3.542$ Å, $\epsilon_{Ar} = 93.3$ K, $\sigma_{C2H5OH} = 4.530$ Å, and $\epsilon_{C2H5OH} = 362.6$ K,[28] where the molecular size of ethanol is considered to be similar to formic acid.

Results and Discussion

Reaction of Formic Acid Dimer. Figure 1 shows a typical IR emission profile at 5.66 μm (upper line) and a pressure transducer signal (lower line) behind the incident shock wave. The emission corresponds to the monomeric formic acid and does not include the contribution from the dimer (the C═O stretching of the dimer encompasses the wavelengths longer than 5.8 μm). The emission intensity rises up abruptly to about a half of the total intensity, and then it increases to a constant level. The initial rise at the shock front is from the original monomer that exists in the mixture at room temperature, and the later increase with time is due to the monomer produced from the dimer dissociation under the incident shock conditions. The rate constant of the dimer dissociation was determined over the temperature range of 700−900 K. Figure 2 shows an Arrhenius plot of the first-order rate constant. The rate is actually constant with a value of 2×10^4 s^{-1} within the experimental

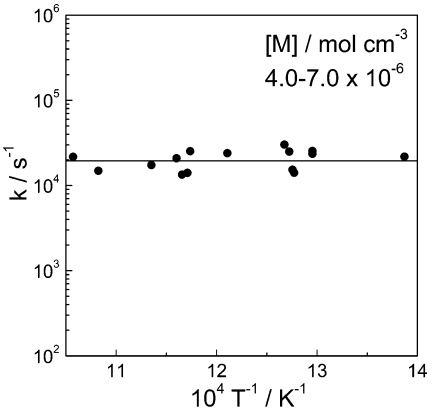

Figure 2. Arrhenius plot of the dissociation rate constant of formic acid dimer.

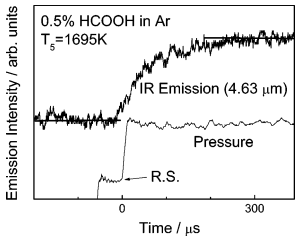

Figure 3. Typical IR emission at 4.63 μm that corresponds to the fundamental band of carbon monoxide. Conditions behind reflected wave are $T_5 = 1695$ K and $\rho_5 = 6.3 \times 10^{-6}$ mol cm^{-3}. R.S. indicates the reflected shock front.

error probably due to a narrow temperature range observed. Since the time resolution of this detection system is on the order of 10^{-5} s, the previous rate may be the lower limit for the dimer dissociation. From the fact that there is no emission (4.63 μm) from carbon monoxide at temperatures lower than 1000 K and that the emission intensity at 5.66 μm monotonically reaches to a constant level, there are no reaction channels to produce other products except for the formic acid monomer. The experiment in the high-temperature region (1300−2000 K), where the dissociation of formic acid is observed, has been done behind the reflected shock waves. Since the time between the arrival of the incident and reflected shock fronts at the observation window is more than 100 μs, the dimer is completely decomposed to the monomer acid until the arrival of the reflected shock front.

Reaction of Formic Acid Monomer. Figure 3 shows a typical emission profile at 4.63 μm. This wavelength includes a fundamental band of CO with a weak contribution from the high levels of CO_2 (ν_2 mode). The time dependent emission intensity, I_t, gives a simple exponential function $(I_\infty - I_t)/I_\infty = \exp(-kt)$, where I_∞ is the intensity obtained after a long reaction time. Thus, we obtained a value of the time constant k in s^{-1} from each profile. Although this time constant actually corresponds to the total decomposition rate constant of the reactant, it is reasonable to postulate that $k_1 \approx k$ under our shock condition where the ratio k_2/k_1 is found to be less than ca. 0.08 (as will be shown in a later paragraph). Figure 4 shows Arrhenius plots of k_1 (upper two lines) with two different total densities by a factor 4. Although the total density of the data point in this figure scatters about 7% over the temperature range, this does not affect the rate parameters meaningfully. As will be described later, the values of k_1 determined in this work excellently agree with the previous experimental results.[5] Theoretical rate constants by the RRKM calculations (dashed lines) are also shown in Figure 4. These are consistent with the experiment, especially

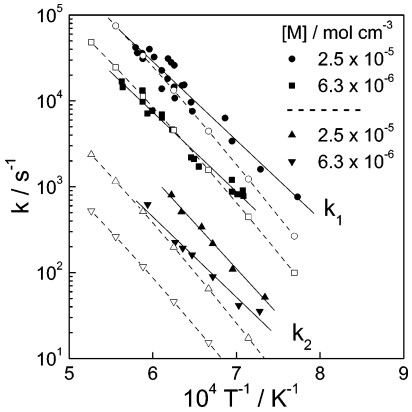

Figure 4. Arrhenius plots of the first-order rate constants k_1 (upper two lines) and k_2 (lower two lines) for the production of CO and CO_2, respectively. The total density [M] is changed by a factor of 4. Further details of k_2 are described in the text. Dashed lines with open symbols designate the unimolecular rate constants by RRKM calculations.

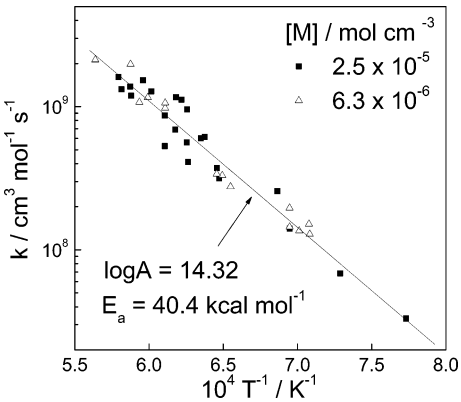

Figure 5. Arrhenius plot of the second-order rate constant k_1. A straight line corresponds to our previous data.

at higher temperature regions. The second-order rate constant $k_{1,0}$ is plotted in Figure 5, where a straight line is the previous experimental data.[5] The Arrhenius expression for the channel 1 is given again by

$$k_{1,0} = 10^{14.32} \exp(-40.4 \text{ kcal mol}^{-1}/\text{RT}) \text{ cm}^3 \text{ mol}^{-1} \text{ s}^{-1} \quad (3)$$

The emission intensity at 4.23 μm (CO_2 ν_3 bands) was so weak within our observed temperature range when it was compared to 4.63 μm that it was difficult to determine the time constant of the initial rise from the emission profile. In the previous experiment,[5] the final product concentration of CO_2 has been measured to be less than 5% of the total reactant concentration, by adding 0.2% CO_2 in the mixture to measure the relative CO_2 yield from the HCOOH pyrolysis.

Next, as a direct emission detecting method, we tried to measure the time-resolved emission intensity at 4.23 μm relative to the reactant concentration. The time-dependent concentrations of CO and CO_2 are expressed by k_1 and k_2 as

$$[\text{CO}] = \frac{k_1}{k_1 + k_2}[\text{HCOOH}]_0[1 - \exp\{-(k_1 + k_2)t\}] \quad (4)$$

and

$$[\text{CO}_2] = \frac{k_2}{k_1 + k_2}[\text{HCOOH}]_0[1 - \exp\{-(k_1 + k_2)t\}] \quad (5)$$

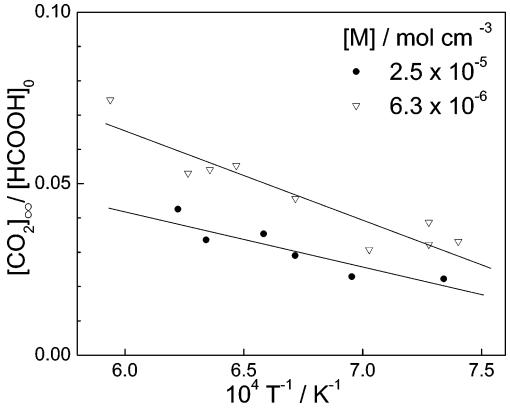

Figure 6. Plot of the ratio $[CO_2]_\infty/[HCOOH]_0$ against the reciprocal temperature. The total density is changed as indicated.

TABLE 1: Arrhenius Parameters for the First-Order Rate Constants k_1 and k_2 at Two Total Densities

total density [M] (mol cm^{-3})	k_1		k_1	
	A (s^{-1})	E_a (kcal mol^{-1})	A (s^{-1})	E_a (kcal mol^{-1})
2.5×10^{-5}	7.45×10^9	41.2	3.02×10^9	48.6
6.3×10^{-6}	2.88×10^9	42.4	1.60×10^8	43.3

Here, we have the following relation at any reaction time:

$$k_2 = k_1 \frac{[CO_2]}{[CO]} \tag{6}$$

The emission of 4.23 μm provides basically the same profile as that of 4.63 μm. However, the intensity of the former was too weak to measure the rate constant from the profile. Therefore, to obtain enough intensity, the slit on the window had to be widely opened by the sacrifice of the time resolution. Accordingly, the ratio

$$\frac{[CO_2]_\infty}{[CO]_\infty} \approx \frac{[CO_2]_\infty}{[HCOOH]_0}$$

was determined after a long reaction time by changing the temperature and total density as shown in Figure 6. A calibration curve of the emission intensity versus the concentration of CO_2 was made in a parallel experiment with CO_2/Ar mixtures. As can be seen from Figure 6, the fraction of CO_2 depends on the total density, that is, it decreases with increasing total density with a slight temperature dependence. This tendency is different from the case at 4.63 μm (CO bands) where the relative intensity to $[reactant]_0$ was constant regardless of the total density. Thus, we can determine the rate constant for channel 2 by the relation $k_2 = k_1[CO_2]_\infty/[CO]_\infty$ from eq 6. Arrhenius plots of the first-order k_2, which show a different density dependence from that of k_1, are also included in Figure 4. Arrhenius parameters for each line in Figure 4 are summarized in Table 1. From this table, it appears that the activation energy for k_1 is constant around 41.5 ± 1 kcal mol^{-1} regardless of the total density, while that for k_2 varies from 43 to 49 kcal mol^{-1} by changing the density by a factor of 4. This difference in the activation energy against the total density suggests that these two channels are in different pressure regimes. The theoretical rate constants for k_2 are also shown in Figure 4. When they are compared with the case of channel 1, experimental rate constants for channel 2 are quite different from the theoretical rates. Because direct observation of the rate constants for channel 2 was very hard due to the low concentration of CO_2, the present experimental rates could be regarded as the upper limit of channel 2. Figure 7 shows logarithmic plots of the rate constants k_1 and k_2 against the total density at 1500 K. The data points of the previous experiments[5] are also included in the k_1 plot. A solid line indicated on the k_1 plot has a gradient of one (i.e., $k_1(s^{-1})$ is proportional to [M] (mol cm^{-3})). Although number of the data points is limited for the k_2, a gradient of the k_2 line is found to be smaller than one. It appears that the rate of the channel 1 is second-order, and channel 2 is in the falloff region under the present experimental conditions. The theoretical rate constants k_1 and k_2 against the total density at 1500 K are also shown in Figure 7. It is noted that calculated rate constants are almost parallel with each other and that both slopes are smaller than one. We checked the theoretical k_1 and k_2 values in a wider pressure range and found that the RRKM rates for both the channels 1 and 2 are in the falloff region.

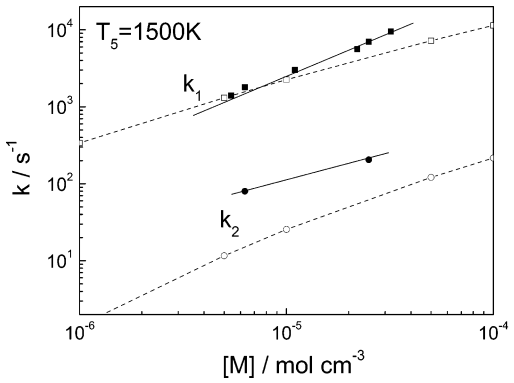

Figure 7. Logarithmic plots of the first-order rate constants k_1 and k_2 and the total density at 1500 K. Results of k_1 include the previous data. Dashed lines with open symbols designate the unimolecular rate constants by RRKM calculations.

In the present study, another experiment was performed using the magic-hole type shock tube. The product distributions against the temperature for the test gas mixtures, 1% HCOOH in Ar and 4% HCOOH in Ar, are shown in Figure 8. Under our experimental conditions, the observed products were CO, H_2, and CO_2. The CO_2 concentration was much lower than CO and less than 5% of the total reactant concentration. This small fraction of CO_2 production is essentially in agreement with our previous conclusions. Simulation results (solid curves in Figure 8) by using $k_1 = 2.3 \times 10^{15}$ exp(−50 kcal mol^{-1}/RT) cm^3 mol^{-1} s^{-1} and $k_2 = 1.4 \times 10^{15}$ exp(−57 kcal mol^{-1}/RT) cm^3 mol^{-1} s^{-1} may reproduce the product distribution. Here, the k_1 value is taken from that of Hsu et al.,[4] but the k_2 value is adjusted as about 1/11 of that by Hsu et al. Figure 8 also shows the results calculated using $2k_1$ (dotted curves) and $0.5k_1$ (broken curves). When $k_1 = 2.3 \times 10^{15}$ exp(−50 kcal mol^{-1}/RT) cm^3 mol^{-1} s^{-1} and $k_2 = 1.5 \times 10^{16}$ exp(−57 kcal mol^{-1}/RT) cm^3 mol^{-1} s^{-1} reported by Hsu et al.[4] were used, the calculated CO_2 (broken curves) is significantly larger than the observed concentration.

It was once suggested by Fransisco[13] that the low concentration of CO_2 in our previous experiment was attributed to the selective quenching of the emission from CO_2 in formic acid. However, the explanation is inconsistent with the present experimental results. It is thus undoubtedly clear that channel 2 to produce CO_2 is not as important as channel 1.

What Is the Cause of the Difference between the Two Channels? The present experiment verified the validity of the previous experimental results and is basically consistent with other experimental results, except for the conclusion of ref 4 that the rates for the two decomposition channels are comparable. In our previous paper on formic acid decomposition,[5] the

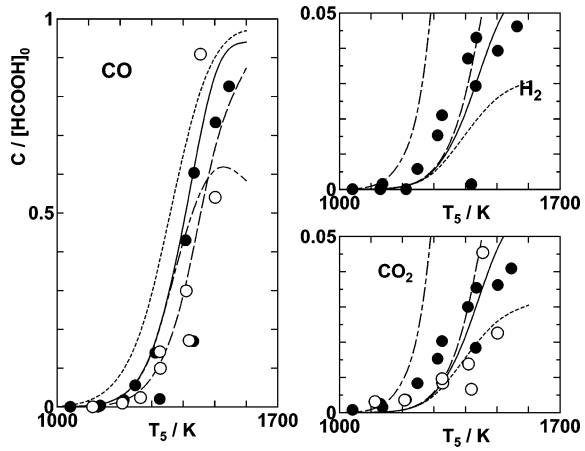

Figure 8. Product distributions behind reflected shock wave observed with mixtures, 1% HCOOH in Ar (○) and 4% HCOOH in Ar (●). $[HCOOH]_0$ is the initial concentration of formic acid, and C is the concentration of products after the effective heating time t_e at temperature T_5. The total pressure and density ranges are 1.2−2.4 atm and 1.3×10^{-5} to 1.9×10^{-5} mol/cm^3, respectively. Solid curve corresponds to the calculated using $k_1 = 2.3 \times 10^{15}$ exp(−50 kcal mol^{-1}/RT) cm^3 mol^{-1} s^{-1} and $k_2 = 1.4 \times 10^{15}$ exp(−57 kcal mol^{-1}/RT) cm^3 mol^{-1} s^{-1}; dash−dotted curve corresponds to the calculated using $k_1 = 2.3 \times 10^{15}$ exp(−50 kcal mol^{-1}/RT) cm^3 mol^{-1} s^{-1} and $k_2 = 1.5 \times 10^{16}$ exp(−57 kcal mol^{-1}/RT) cm^3 mol^{-1} s^{-1} reported by Hsu et al.[4] Dotted curve corresponds to the calculated using $k_1 = 4.6 \times 10^{15}$ exp(−50 kcal mol^{-1}/RT) cm^3 mol^{-1} s^{-1} and $k_2 = 1.4 \times 10^{15}$ exp(−57 kcal mol^{-1}/RT) cm^3 mol^{-1} s^{-1}. Broken curve corresponds to the calculated using $k_1 = 1.7 \times 10^{15}$ exp(−50 kcal mol^{-1}/RT) cm^3 mol^{-1} s^{-1} and $k_2 = 1.4 \times 10^{15}$ exp(−57 kcal mol^{-1}/RT) cm^3 mol^{-1} s^{-1}.

difference in the activation energy for the two channels was estimated to be about 20 kcal mol^{-1} using ab initio calculations at the MP2/6-31G//HF/6-31G level. Since polarization functions were not included at the stage of geometry optimization, the rough barrier heights resulted in a large difference between the two channels. However, potential energy barriers for the transition states of the two channels were recently recalculated to be 63.4 kcal mol^{-1} for channel 1 and 66.3 kcal mol^{-1} for channel 2, respectively, with the zero-point energy correction at the MP4/cc-pVQZ//B3LYP/cc-pVTZ level.[14] These values are in good agreement with those of other investitations.[10−13] Then, what is the cause of the difference in the rates between the two channels? To find the answer for this question, the rate constants for the two channels were examined on the basis of thermochemical considerations using conventional transition state theory (CTST), and the ratio of k_2/k_1 was also evaluated at several temperatures. For the other estimation of rate constants, RRKM calculations were performed under our experimental conditions to examine their pressure dependence. As is generally known, the rate constant for the high-pressure limit corresponds to that of the CTST.

The results for three experimental and two theoretical analyses are compared in Table 2. Here, we obtained the comparable results for the k_2/k_1 ratio of 0.03 to ∼0.07 from both calibrated IR emission intensity and product analysis of the shock-heated gas. On the other hand, the k_2/k_1 ratios from ref 4 are significantly larger than those of the present work. The ratios calculated from CTST are also smaller than 1 primarily due to the difference in the entropy of activation $\Delta S^{\ddagger}$ for the two channels, for example, $\Delta S^{\ddagger}$ is 4.71 cal mol^{-1} K^{-1} for channel 1 and −0.43 cal mol^{-1} K^{-1} for channel 2 at 1500 K, respectively. It should also be noted that the difference of the potential barrier heights (ca. 3 kcal mol^{-1}) is less important in determining the branching ratio for two channels. Furthermore,

TABLE 2: Comparison of k_2/k_1 Ratios at Several Temperatures

T (K)	exp 1[a]	exp 2[b]	exp 3[c]	calc 1[d]	calc 2[e]
1400	0.028	0.048	0.53	0.034	0.014
1500	0.034	0.057	0.63	0.036	0.015
1600	0.039	0.065	0.72	0.038	0.015

[a] This paper (emission measurements). These values were obtained from Arrhenius parameters of Table 1 at a total density of 2.5×10^{-5} mol cm^{-3}. [b] This paper (product gas analysis). Rate constants obtained in Figure 8 were used, that is $0.09 \times k_2/k_1$(exp 3). [c] Ref 4. [d] This paper. Rate constants for two channels were estimated from the conventional transition state theory using the parameters given by the MP4/cc-pVQZ//B3LYP/cc-pVTZ level. [e] This paper. Rate constants for two channels were estimated from the RRKM calculations using the parameters given by the MP4/cc-pVQZ//B3LYP/cc-pVTZ level.

the ratios by the RRKM calculations are also consistent with the experimental values within a factor of 2 except for weak sensitivity on the temperature, indicating that the difference of two theoretical rate constants is enhanced by the fact that decomposition of formic acid is in the falloff region under the experimental conditions of the present study. The inconsistence with the experimental values may be caused by the inadequacy of some empirical parameters used in the RRKM calculations. To our knowledge, it is the first observation that the two channels proceed with different pressure dependences in multichannel (parallel) reactions. In acetic acid, the two competing channels actually proceed with the same rate under the same pressure dependence.[29,30]

Conclusion

The thermal decomposition of formic acid was reinvestigated in the temperature range of 1000−2000 K and in the density range of $(0.5-2.5) \times 10^{-5}$ mol cm^{-3} using two shock tubes. Results showed that the main channel is the dehydration to produce H_2O and CO, and the decarboxylation to produce CO_2 and H_2 occurs as a minor channel. The present results strongly support the data of our previous experimental investigation. We also found that the dehydration process behind the present shock conditions takes place in the second-order region, but on the other hand, the decarboxylation is in the falloff region. Significantly lower values for the experimental k_2/k_1 ratio than those by Hsu et al. were actually supported from the present CTST and RRKM calculations.

Acknowledgment. This work is dedicated to the memory of Prof. K. Saito. This paper is the last report written by him, as he died on May 20, 2004. The authors thank Prof. K. Okada and Dr. Y. Kohno for their helpful discussions.

References and Notes

(1) Blake, P. G.; Hinshelwood, C. *Proc. R. Soc. London, Ser. A* **1960**, *255*, 444.

(2) Benson, S. W.; O'Neal, H. E. *Kinetics on Gas-Phase Unimolecular Reaction, National Standards of Reference Data Series National Bureau of Standards 21*; U.S. GPO: Washington, DC, 1970; p 111.

(3) Blake, P. G.; Davies, H. H.; Jackson, G. *J. Chem. Soc.* **1971**, 1923.

(4) Hsu, D. S. Y.; Shaub, W. M.; Blackbaum, M.; Lin, M. C. *The Nineteenth International Symposium on Combustion*; The Combustion Institute: Pittsburgh, PA, 1983; p 89.

(5) Saito, K.; Kakumoto, T.; Kuroda, H.; Torii, S.; Imamura, A. *J. Chem. Phys.* **1984**, *80*, 4989.

(6) Samsonov, Y. N.; Petrov, A. K.; Baklanov, A. V.; Vihzin, V. V. *React. Kinet. Catal. Lett.* **1976**, *5*, 197.

(7) Evans, D. K.; McAlpine, R. D.; McClusky, F. K. *Chem. Phys.* **1978**, *32*, 81.

(8) Corkum, R.; Willis, C.; Back, R. A. *Chem. Phys.* **1977**, *24*, 13.

(9) Yamashita, K.; Yamabe, T. *Int. J. Quantum Chem. Symp.* **1983**, *17*, 177.
(10) Ruelle, P.; Kesselring, U. W.; Ho, N.-T. *J. Am. Chem. Soc.* **1986**, *108*, 371.
(11) Ruelle, P. *J. Am. Chem. Soc.* **1987**, *109*, 1722.
(12) Goddard, J. D.; Yamaguchi, Y.; Schaefer, H. F., III. *J. Chem. Phys.* **1992**, *96*, 1158.
(13) Francisco, J. S. *J. Chem. Phys.* **1992**, *96*, 1167.
(14) Takahashi, O.; Itoh, K.; Kawano, A.; Saito, K. *J. Mol. Struct. (THEOCHEM)* **2001**, *545*, 197.
(15) Kurosaki, Y.; Yokoyama, K.; Teranishi, Y. *Chem. Phys.* **2005**, *308*, 325.
(16) Tokmakov, I. V.; Hsu, C.-C.; Moskaleva, L. V.; Lin, M. C. *Mol. Phys.* **1997**, *92*, 581.
(17) Wang, B.; Hou, H.; Gu, Y. *Chem. Phys.* **1999**, *243*, 27.
(18) Wang, B.; Hou, H.; Gu, Y. *J. Phys. Chem.* **2000**, *104*, 10526.
(19) Saito, K.; Shiose, T.; Takahashi, O.; Itoh, K.; Kawano, A.; Okada, K.; Tabayashi, K. *Proceedings of the 23rd International Symposium on Shock Waves*; Lu, F., Wars, F., Eds.; Springer−Verlag: New York, 2001; p 293.
(20) Hidaka, Y.; Shiba, S.; Takuma, H.; Suga, M. *Int. J. Chem. Kinet.* **1985**, *17*, 441.
(21) Hidaka, Y.; Nakamura, T.; Miyauchi, A.; Shiraishi, T.; Kawano, H. *Int. J. Chem. Kinet.* **1989**, *21*, 643.
(22) Hidaka, Y.; Hattori, K.; Okuno, T.; Inami, K.; Abe, T.; Koike, T. *Combust. Flame* **1996**, *107*, 401.
(23) Hidaka, Y.; Henmi, Y.; Ohonishi, T.; Okuno, T. *Combust. Flame* **2002**, *130*, 62.
(24) Hidaka, Y.; Takahashi, S.; Kawano, H.; Suga, M.; Gardiner, W. C., Jr. *J. Phys. Chem.* **1982**, *86*, 1429.
(25) Chase, M. W., Jr.; Davies, C. A.; Downey, J. R., Jr.; Frurip, D. J.; McDonald, R. A.; Syverud, A. N. *J. Phys. Chem. Ref. Data, Suppl.* **1995**, *14*, 1.
(26) Burcat, A. "Third Millennium Ideal Gas and Condensed Phase Thermochemical Database for Combustion"; ftp://ftp.technion.ac.il/pub/supported/aetdd/thermodynamics.
(27) Gilbert, R. G.; Smith, S. C. *Theory of Unimolecular and Recombination Reactions*; Blackwell Scientific Publications: Oxford and Cambridge, 1990.
(28) Reid, R. C.; Prausnitz, J. M.; Poling, J. E. *The Properties of Gases and Liquids*, 4th ed.; McGraw-Hill: New York, 1987.
(29) Takahashi, O.; Itoh, K.; Saito, K. *J. Mol. Strct. (THEOCHEM)* **2002**, *584*, 249.
(30) Mackie, J. C.; Doolan, K. R. *Int. J. Chem. Kinet.* **1984**, *16*, 525.